Sensitivity study of resonant τ-sneutrino production in the eμ final state at $\sqrt{s} = 13$ TeV at CMS

von

Christoph Schuler

Bachelorarbeit in Physik

vorgelegt der

Fakultät für Mathematik, Informatik und Naturwissenschaften der RWTH Aachen

im Juli 2015

angefertigt im

III. Physikalisches Institut A

bei

Prof. Dr. Thomas Hebbeker

Acknowledgement

At this point, I want to give thanks to:

My surveyors Prof. Dr. Thomas Hebbeker and Prof. Dr. Christopher Wiebusch for reading and evaluating this work.

All people at the III. Physikalischen Institut A, who have been very helpful when I had problems and who gave useful tips to improve this work.

My tutors Thomas Esch and Sören Erdweg for their patience and attentiveness. Whenever I had a question or problem, they discussed it with me, until we found a solution.

My family for their moral support they always give me.

Thank You!

Eidesstattliche Erklärung

Hiermit erkläre ich, Christoph Schuler, an Eides statt, dass ich die vorliegende Bachelorarbeit selbstständig verfasst und keine anderen als die angegebenen Quellen und Hilfsmittel benutzt habe.

Aachen,

Abstract

This thesis is done in preparation of an analysis for future resonant τ-sneutrino searches with an electron and a muon in its final state in proton-proton collisions at the LHC at CERN with a center-of-mass energy of 13 TeV and a luminosity of 1 fb^{-1}. The underlying theory for this search is the theory of supersymmetry with R-parity violation. As backgrounds, the Diboson backgrounds, the $t\bar{t}$ background, the tW background and the Drell-Yan background are relevant and taken from Monte Carlo. Additionally, the jet background is considered and estimated in this work. With signal samples from Monte Carlo, the mass resolution and efficiencies are determined for 13 TeV data. At the end, a expected limit is set for the τ-sneutrino mass.

Contents

1 Introduction and Theory

1.1 Standard Model of Particle Physics

Physicists have collected their understanding of the smallest particles in the so called Standard Model of Particle Physics (SM). It describes the electromagnetic, the strong and the weak interaction, but not the gravitational one (which is one of the model's weaknesses). Additionally, it classifies all known subatomic particles. All matter around us is made of only three different particles (the electron, the up and the down quark), but in time, scientists have found additional particles which can be classified as shown in Fig. 1.

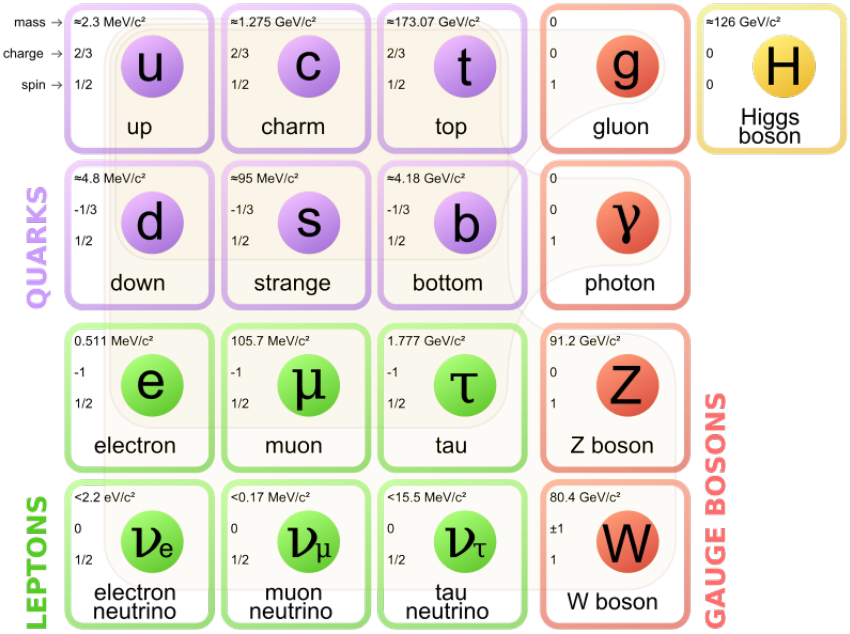

Figure 1: Basic particles in the Standard Model of Particle Physics with fermions divided into three generations (columns), the gauge bosons in the fourth column and the Higgs boson in the fifth [3].

All these particles are defined by their interactions they have with other particles, and they are divided into two groups defined by their spin. There are the twelve particles called fermions with halfinteger spin (three columns on the left in Fig. 1) and the bosons with integer spin, which include four force mediator particles and the Higgs boson, which gives the masses to the particles. Additionally, to each fermion there is a corresponding antiparticle with the same mass but reversed signs in all other quantities (like electric charge, weak isospin etc.).

Fermions are additionally divided into two groups, the quarks (on the top of Fig. 1) and the leptons (on the bottom of Fig. 1). Pairs in columns of those form generations (e.g. up- and down quark are first-generation quarks), which exhibit similar physical behavior. The group

of quarks consists of six particles (up and down, charm and strange, top and bottom). The defining property of quarks is the fact that they are the only fermions which carry color charge and therefore interact via the strong interaction. As quarks carry a thirdinteger electric charge and weak isospin as well, they also interact via the electromagnetic and the weak interaction. Additionally, each quark is assigned the baryon number 1/3 and each antiquark the baryon number -1/3.

The upper line of the leptons, namely the electron, the muon, and the tau, are called "charged leptons", as they all have the electric charge -1, but no color charge, so they interact via the electromagnetic force. They also carry weak isospin so they also interact via the weak interaction. To each charged lepton there is a corresponding neutrino which carries no electric charge, but weak isospin, and hence only interacts via the weak interaction, which results in very rare detections of these neutrinos due to their small interaction rate. To each lepton, there is a charge-like lepton number l assigned, which counts the members of same generation letpons (e.g. the electron neutrino has an electron number of 1, a muon number and a tau number of 0). Similarily, each antilepton has a negative lepton number.

Each generation member has a greater mass then the corresponding particles of lower generation and therefore can decay into these (backward way is impossible due to energy conservation). This possibility does not hold true for the neutrinos, as they do not decay. As a decay of a first generation fermion has not been measured yet, it is supposed that they do not decay, and therefore, all matter we interact in daily life exists out of these particles.

On the right side in red (Fig. 1), there are the gauge bosons, which carry the forces of the interaction. In the SM, forces are described as an exchange of particles.

The photon is a massless particle and mediates the electromagnetic force between electrically charged particles. This force is well-described by the quantum electrodynamics (QED) and its strength is of the order of 10^{-2} relative to the strong interaction.

Then, as mediator of the strong interaction, there is the gluon. As the only force mediator, the massless gluons themself carry the charge they interact with, always one color charge (red, green, blue) and one anticolor charge, so there would be 9 gluons in total, but due to the fact, that long-range gluon interactions do not exist, the singlet state does not exist, so there are 8 different gluons. Due to this charged force mediator, there is selfcoupling of the gluons. So, when quarks bound by gluons are stretched apart by force (through collision), gluons are created until they can actually form color-charge neutral particles as then the gluons are in a bound state again and the "hadronisation", as this process is called, is finished and only the remaining color neutral hadrons remain. They bind together to a color-neutral particle (hadron) which consist of either a quark and its antiquark (then it is called meson), or three quarks (called baryon). The fact that particles with color charge do not exist isolatedly is called confinement and results from the fact that the potential of the strong interaction becomes linear for high distances.

The massive W and Z gauge bosons mediate the weak interaction between particles of different flavors (all fermions). Its strength is, due to the high mass of its mediating particles, relatively small in comparison with the other forces. The weak interaction is the only force which is able to change flavors of particles (like in the β-decay) aswell as violating parity (P), charge conjugation (C), time conjugation (T) and the combination of parity and charge conjugation (CP).

From a mathematical point of view, the interactions can be specified in symmetry groups.

This part is closely oriented on the script from the lectures in [18].

Mathematically, the electromagnetic interaction is described by the $U(1)$-group with one boson as force mediator, the strong interaction (with its three colors and eight gluons) is described by the $SU(3)$-group and the weak interaction is described by the $SU(2)_L$-group. Here, the index L means, that only lefthanded particles interact with the W boson, which means particles, whose momentum direction is opposed to the direction of the projection of the spin on the momentum. So all in all, the SM has a $SU(3)\times SU(2)\times U(1)$-symmetry.

In all interactions in the SM, energy, momentum, charge, baryon number B and lepton number are conserved. Additionally, the CPT symmetry is conserved, which means that for any allowed process, if the signs of the charge, of the parity (location) and of the time are reversed, it is again an allowed process in the SM. All these lower symmetries are otherwise only indiviually conserved in the electromagnetic and strong interaction but not in the weak interaction.

In the SM, all particles are massless per definition, and their mass is allocated dynamically by the so called higgs-mechanism. Here, a Higgs boson couples on each particle in such a way, that these particles get their mass. Due to the discovery of the Higgs boson in 2012, this mechanism seems to be proven correctly.

But still, there are several difficulties the Standard Model fails to overcome. First of all, as already mentioned, it does not include the description of gravity, for which Einstein's general theory of relativity applies. Additionally, the Standard Model predicts that neutrinos are massless, but due to observed neutrino oscillations (they can change their lepton flavor in flight) it has been stated that they have to have a mass different from zero. Another problem to the Standard Model is the evidence of so called dark matter in the cosmology, for which there is currently no particle in the Standard Model to describe it. A more conceptual, but very serious problem is the hierarchy problem, which poses the question why the weak force is 10^{32} times stronger than gravity, or, more technically the Higgs mass renormalization by various loop diagrams would lead to unacceptable huge Higgs masses [14, 11]. Due to these (and other) concerns, different theories or extensions of the Standard Model, which can solve some of these problems, are made and tested experimentally. One very popular idea is the supersymmetry.

1.2 Introduction into Supersymmetry

1.2.1 General supersymmetry idea

The supersymmetry theory introduces a symmetry between fermions and bosons, so for each fermion in the SM a corresponding supersymmetric boson, and for each boson in the SM a corresponding supersymmetric fermion is predicted. This is in detail for each lepton a 'slepton' (selectron, sneutrinos, etc), for each quark a squark, and for each mediator a corresponding twin (photino, gluino, etc) with spins given in Tab. 1. So far, these particles have not been measured, which implies that supersymmetry is a broken symmetry (otherwise the correspondig superpartners would have the same mass as the corresponding SM particles), but this theory is giving reasonable explanations for various problems the standard model encounters.

Spin	SM particles	Superpartners	Spin
1/2	Leptons (l)	Sleptons ($\tilde{l}$)	0
1	Quarks (q)	Squarks ($\tilde{q}$)	1/2
0	Gluons (g)	Gluino ($\tilde{g}$)	1/2
0	Photons	Photino	1/2
0	Z	Zino	1/2
0	W	Wino	1/2
0	Higgs (H)	Higgsino	1/2

Table 1: Particles and their corresponding superpartners.

These additional particles lead to a unification of the coupling constants of the different forces at a certain point (around 10^{16} GeV). This means, that all forces described by the standard model are just different effects from one single force, which would be a necessity for a unified theory. This is shown in Fig. 2.

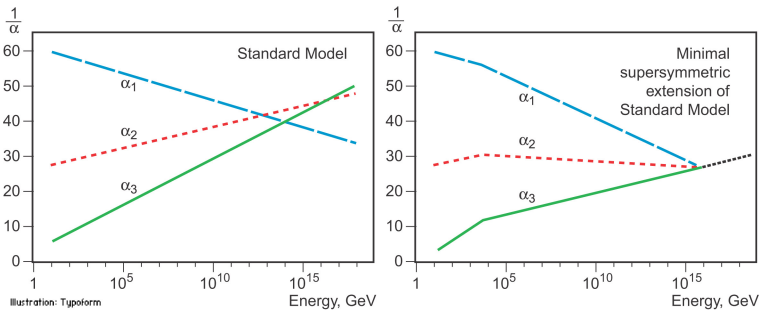

Figure 2: Coupling constants in the Standard Model (left), and its supersymmetric extension (right) [2].

1.2.2 R-Parity violating processes

In some models in the supersymmetry, the proton could decay in about 10^{-2} seconds. But with experiments, scientists determined the lifetime of the proton to be at least bigger than 10^{31} years [10], so the theory has to be modified. To explain these measurements, it is one possibility to introduce the so called R-Parity:

$$R = (-1)^{3(B-L)+S}$$

This R is an additional multiplicative quantum number, where B is the baryon number, L is the lepton number and S is the spin. The value for R is for standard model particles 1 and for the added supersymmetric particles -1. It ensures, that Standard Model particles can only decay into Standard Model particles and likewise for supersymmetric particles. In this case, there has to be a lightest supersymmetric particle (LSP), which cannot decay and therefore is a very interesting candidate for the dark matter (in case it does not carry charge). Additionally, supersymmetric particles can only be created in pairs in interactions with SM-particles [12].

In this analysis, another possibility of explanation of the stability of the proton, the baryon triality is assumed [4]. So, the process of a quark-antiquark pair annihilating, resulting in the

supersymmetric τ-sneutrino which then in turn decays into an electron and a muon is searched for, which would be a lepton number violating process, and therefore a R-Parity violating process. This process is shown graphically in Fig. 3.

This process is by theory only possible with down-like quarks, so exchangebly there could be a strange-antistrange or bottom-antibottom pair annihilating (but down-antidown is most likely). λ'_{311} and λ_{132} are called Yukawa couplings of the interaction, where the indices indicate the generations. So for the creation of the τ-sneutrino from to down quarks, $\lambda'_{311} \neq 0$ has to be fulfilled and for the decay into an electron and a muon, $\lambda_{132} \neq 0$ has to be fulfilled. For this analysis, both of the couplings are set to 0.01 and all other combinations (e.g. λ_{322}) are assumed to be 0. In further analysis, it is possible to search for this process with different couplings. The signature of this signal is the final state of an electron and a muon, which is (in the SM) due to the lepton number conservation, not possible (there would have to be atleast the corresponding neutrinos of the electron and the muon).

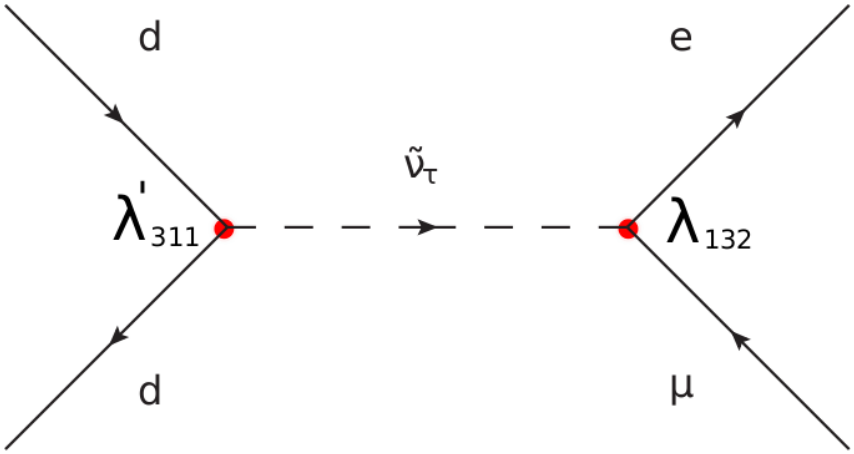

Figure 3: Feynman diagram of R-Parity violating process, signal model. A down-antidown pair annihilate each other. In this process, the supersymmetric τ-sneutrino is created, which quickly decays while giving an electron and a muon. Due to charge conservation (net charge zero before the process), one of those particles should be an antiparticle.

2 Overview on the CMS detector

In this section, the basic quantities referred to in the following analysis will be introduced and a small overview on the CMS (Compact Muon Solenoid) detector is given. All information in this section is taken from [6]. This detector is one of the four big detectors at the Large Hadron Collider (LHC) in CERN, Geneva, a particle collider designed to collide proton beams at a center-of-mass energy of $\sqrt{s} = 14$ TeV. In the upcoming run, where this analysis is made for, the center-of-mass energy will be $\sqrt{s} = 13$ TeV. The CMS detector has a length of 21 m, a width of 15 m and a height of 18 m. It weights around 12.500 tons.

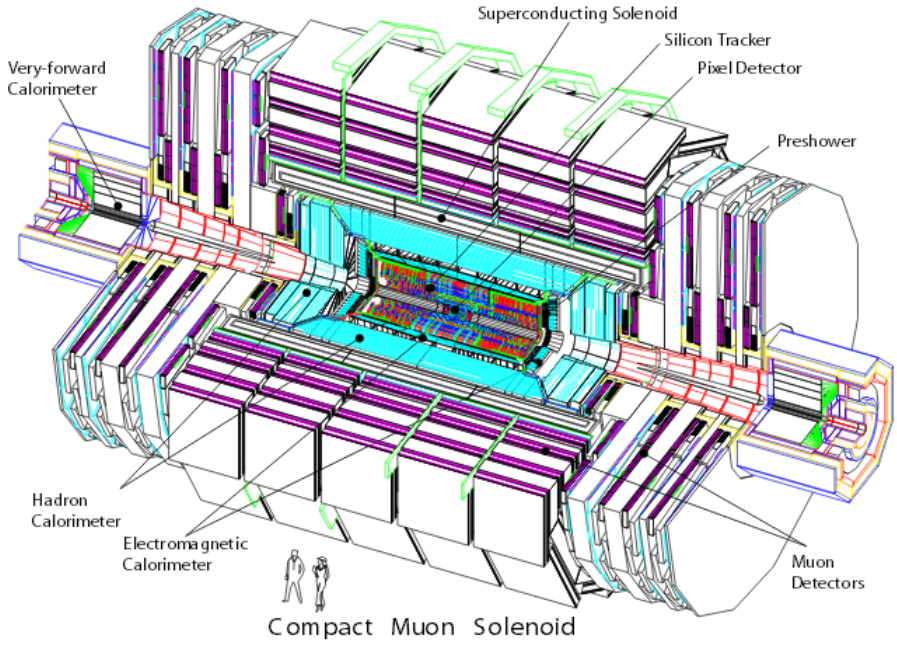

Figure 4: The CMS detector, perspective view [6].

As can be seen in Fig. 4, the CMS detector is structured in several layers around the collision point. Outgoing from there, there is the inner tracker, which records the trajectories of charged particles. It consists of the inner silicon-pixel-detector and the outer silicon-strip-tracker. The pixel-detector has a pixel-width of 100 Å - 150 µm and has for measurements in radial direction a resolution of 10 µm. Due to the proximity to the beam, it is very important for the identification of particles, which decay shortly after their creation (like b and c quarks). The strip-detector consists of several layers, divided into strips to measure the radial direction. With this, it is possible, to get a very good track reconstruction of high energy leptons.

The next layer is the electromagnetic calorimeter (ECAL), which measures the energy of particles electromagnetically interacting like photons and electrons. It consists of more than 80.000 $PbWO_4$-crystals and a corresponding photodetector and is divided into a central barrel and the endcaps. It is surrounded by the hadronic calorimeter (HCAL), which measures the hadronic components of the decays like protons, neutrons and pions. The most part of it is in the inner of the magnet and consists of brass and scintillator-material. A part of it is around the magnet (outer HCAL (HO)) and is used for a better energy resolution in the central area. The strong, superconducting solenoid-magnet, which surrounds all of the previous (but the HO), is (so far) the biggest solenoid ever built. It is cooled to around 3 K and can create a magnetic field up to 3.8 T. Around the solenoid is a iron yoke, which closes the magnetic field lines and therefore deflect the muons in order to measure the bend of their track.

A very important part of the detector is the muon system, which measures the bending angle of the muons what from their respective momentum can be calculated. The muon system is segmented in the barrel and the endcap region. In the central barrel region, drift chambers with

rectangular drift cells are used. If a muon passes such a cell, the muon ionizes the containing mixture of gases (85% Ar, 14% CO_2), and its passing position can be evaluated as exactly as 200 µm. In the two endcap regions, where the magnetic field is uneven and the particle rates are higher, the muon system consists of cathode strip chambers. As only muons, neutrons and possibly neutrinos are able to reach the muon system (other particles decay earlier or are absorbed by the detector), and of those the muons are the only particles which are charged and therefore deflected, their momentum can be measured by the bend of the track [1].

This setup is used to have good muon identification and momentum resolution over a wide range of momenta and angles, good charged-particle momentum resolution and reconstruction efficiency in the inner tracker (e.g. for muons and electrons), as well as good electromagnetic energy resolution and efficient photon and lepton isolation at high luminosities. For muons, the momentum resolution at hight momenta (1 TeV) is about 5%, whereas for electrons an energy resolution of 0.5% for 120 GeV has been attained.

In the following, the most important quantities are defined. By convention, the CMS coordinate system is oriented such that the x-axis points to the center of the LHC ring (south), the y-axis points vertically upward and the z-axis is in the beam direction (to the west).

The transversal momentum is the momentum transverse to the beam direction and is computed from the x and y component. The so called pseudorapidity is defined as

$$\begin{aligned} \eta &= -\ln(\tan(\theta/2)) && (1)\\ &= \operatorname{artanh}(p_L/|\vec{p}|) && (2) \end{aligned}$$

where p_L is the momentum in the direction of the beam pipe and θ is the angle between the z-axis and the particle trajectory. Additionally, there is the azimuthal angle ϕ around the beam pipe (in the xy plane). Then, as η and ϕ are orthogonal, you can define a distance ΔR between two particles, which is given by

$$\Delta R = \sqrt{(\Delta\eta)^2 + (\Delta\phi)^2} \tag{3}$$

where $\Delta\eta$ and $\Delta\phi$ are the relative angles of the particles. Additionally, there is the transverse energy E_T given by

$$E_T = E \cdot \sin(\theta) \tag{4}$$

and the very important quanitity of the invariant mass, given as

$$M = \sqrt{(\sum E_i)^2 - (\sum \mathbf{p_i})^2} \tag{5}$$

where it is added over all particles which are (e.g.) part of the decay.

3 Event selection

In this section, the identification cuts the two leptons have to fulfill in order to be accepted are described. Additionally, the signal acceptance is looked at with all efficiencies of the different cuts which are applied on candidate events.

3.1 Particle identification

3.1.1 Muon Identification

In order to select the muons, the high-p_T-muon ID (recommended for use of $p_T > 200$ GeV) is used, which is the same as for the first run. It has the following requirements [16, 4]:

- The muon candidate is reconstructed as a global muon. A global muon is a muon that has a reconstructed trajectory in the muon chambers and in the inner tracking system [8].
- In the global-muon track fit, at least one muon chamber hit has to be included, in order to supress hadronic punch-through and muons from decays in flight.
- In order to to make the selection consistent with the logic of the muon trigger, there have to be muon segments in at least two muon stations. This also suppresses the punch-through and accidental track-to-segment matches.
- The relative error in p_T of the muon best track must be lower than 30% in order to reduce misreconstruction.
- The transverse impact parameter d_{xy} of the muon with respect to the primary vertex has to be smaller than 2 mm and the longitudinal distance of the tracker track d_z with respect to the primary vertex has to be smaller than 5 mm. This is demanded in order to supress the influence of cosmic muons as well as to further suppress the muons from in-flight decays.
- In order to further supress the muons from decays in flight, at least one pixel has to be hit.
- To ensure a good p_T measurement, only those muons are selected, whose number of tracker layers with hits is greater than 5.

3.1.2 Electron Identification

The high-p_T electrons in Spring14 samples are selected with the HEEP 5.1 cuts [13]. They are shown in Tab. 2.

Variable	Barrel	Endcap
E_T	$>$ 35 GeV	$>$ 35 GeV
η range	$\lvert\eta_{SC}\rvert < 1.4442$	$1.566 < \lvert\eta_{SC}\rvert < 2.5$
isEcalDriven	=1	=1
$\lvert\Delta\eta_{in}\rvert$	$<$ max(0.016-$E^{-4}E_T$, 0.004)	$<$ max(0.015 $-$ 8.5$E^{-5}E_T$, 0.006)
$\lvert\Delta\phi_{in}\rvert$	$<$ 0.06	$<$ 0.06
H/E	$<$ 2/E + 0.05	$<$ 12.5/E + 0.05
$\sigma_{i\eta i\eta}$	n/a	$<$ 0.03
E^{2x5}/E^{5x5}	$>$ 0.94 OR $E^{1x5}/E^{5x5} > 0.83$	n/a
EM+Had Depth 1 Isolation	$<$ 2+0.03*E_T+0.28ρ	$<$2.5+0.28ρ for $E_T<$59 else
		$<$2.5+0.03*(E_T-50)+0.28ρ
Track Isolation: Trk Pt	$<$ 5 GeV	$<$ 5 GeV
missing hits	$<=$ 1	$<=$ 1
|dxy|	$<$ 0.02	$<$ 0.05

Table 2: Official HEEP Selection v5.1

E_T, η are defined as in Section 2, H/E is the ratio of the energy departed in the hadronic calorimeter (in a cone with radius 0.15 centered around the electron's position in the calorimeter) to the electromagnetic energy of the electron's cluster in the ECAL (called supercluster). η_{SC} is the pseudorapidity of the electrons supercluster. $|\Delta\eta_{in}|$ and $|\Delta\phi_{in}|$ both describe the corresponding difference of the track position extrapolated to the interaction vertex and the track position extrapolated to the calorimeter (so they make sure, that the two measured tracks are so close to another that they are accepted as from the same particle). $\sigma_{i\eta i\eta}$ is a measure of the spread in η in units of crystals of the electrons energy in the 5x5 block around the seed crystal. The isolation variables ensure, that the electron track is distanced to other tracks to ensure a good measurement and reduce jets faking the electron.

3.2 Signal acceptance

For this analysis, there is are two different trigger used, namely the HLT_Mu50_v1 trigger for the Spring15 samples and the HLT_Mu40_v1 trigger for the Phys14 samples. These trigger cut on muons with a transversal momentum which is at least 50 GeV (40 GeV). The efficiency (defined as in Eq. 6) of the latter is shown in Fig. 5. As it can be seen, the trigger has a small turn on, it does not cut all muons with p_T less than 50 GeV. For muons with higher p_T the efficiency is stable around 90%. In the $\eta - \phi-$plot, the several muon chambers in the first layer of the muon system in the barrel are visible, as there is an efficiency drop at those points, where the several chambers are next to each other. The fact, that different triggers are used for the different sample does not change the outcome, as the preanalysis cut for the muons is on $p_T > 55$ GeV.

$$\epsilon_{Trigger} = \frac{N(Muon\,ID + Trigger)}{N(Muon\,ID)} \quad (6)$$

$$\epsilon_{RECO} = \frac{N(reconstructed\,lepton)}{N(generated\,lepton)} \quad (7)$$

$$\epsilon_{ID} = \frac{N(reconstructed\,lepton + ID)}{N(reconstructed\,lepton)} \quad (8)$$

To accept a muon / electron candidate to be reconstructed, the particle has to lie within a cone of $\Delta R = 0.5$ with the generated particle. In case there are more possible candidates for the reconstruction, the closest one is selected. The reconstrucion efficiency, defined as in Eq. 7, is evaluated for all lepton candidates and additionally for all candidates in their corresponding acceptance, shown in Fig. 6 and 7. The acceptance cuts are shown in Tab. 3. For the plot of the efficiency as a function of p_T, there is no cut on the transverse momentum. As can be seen, the efficiency is rather low for $p_T < 50$ GeV but then becomes very good for high-p_T particles.

	p_T	η
Muon	>55	<2.1
Electron	>35	<2.5

Table 3: Preanalysis cuts on muons and electrons

Afterwards it is looked for these particle candidates to fulfill their respective ID given in Section 3.1. The efficiency of the ID Cut defined in Eq. 8, is evaluated for all candidates and additionally all candidates in their respective acceptance aswell. It is shown in Fig. 8 and 9, also here, in the efficiency as a function of p_T, there is no cut on the transverse momentum.

The events have to have at least one selected electron and one selected muon; in case there are several of those, the pair with the highest invariant mass is chosen for the analysis. Additionally a cut on opposite-sign charge events, a b-jet veto and a cut on $\Delta\phi > 2.7$ can be applied. The RPV signal's acceptance times efficiency is shown in Fig. 10. After a turn-on up to $M_{\tilde{\nu_\tau}} \approx 800$ GeV, it stabilizes around 70%. For the limit setting at arbitrary signal masses, a fit is performed to the distribution:

$$A \cdot \epsilon(M) = 0.92 - \frac{272}{262 + M/\mathrm{GeV}} - 2.38 \cdot 10^{-5} M/GeV \quad (9)$$

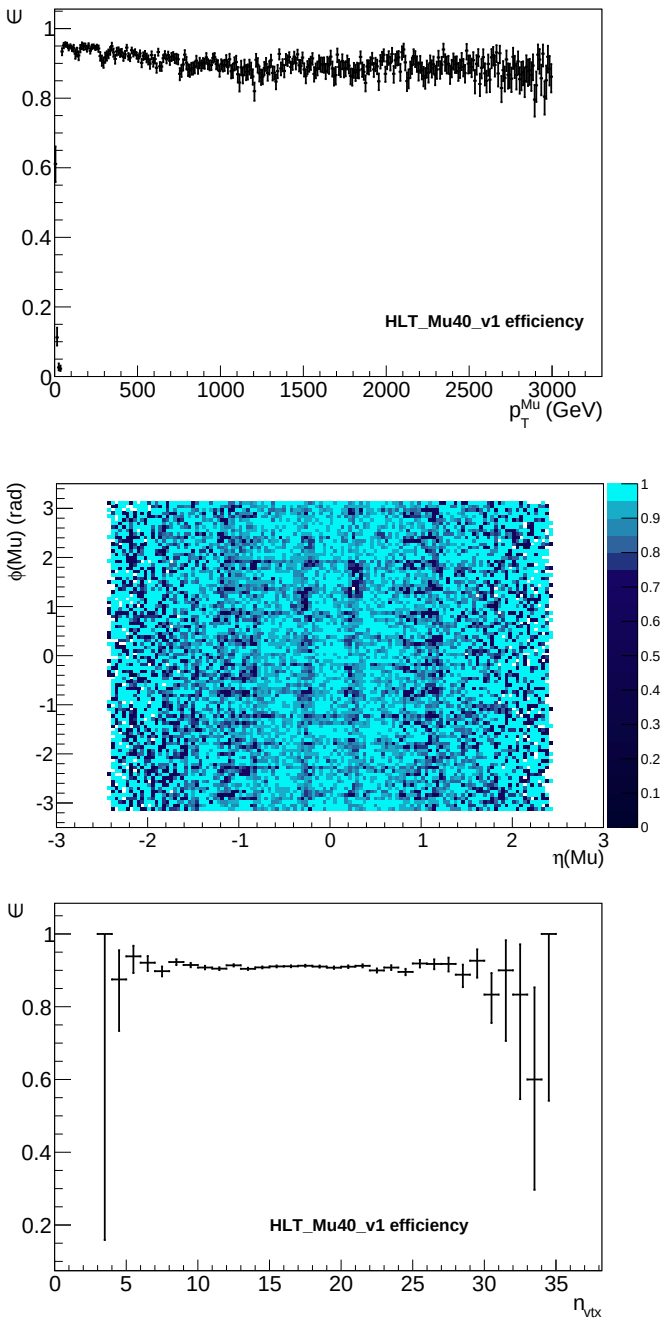

Figure 5: Trigger efficiency of the HLT_Mu40_v1 trigger. The efficiency is fairly constant around 90% for high-p_T muons (on the top). The Number of Vertices-distribution (bottom) shows no features, as expected. The structure in the $\eta - \phi$−plot (in the middle) represents the points, where first layer muon chambers are next to each other, so the detection is slightly worse.

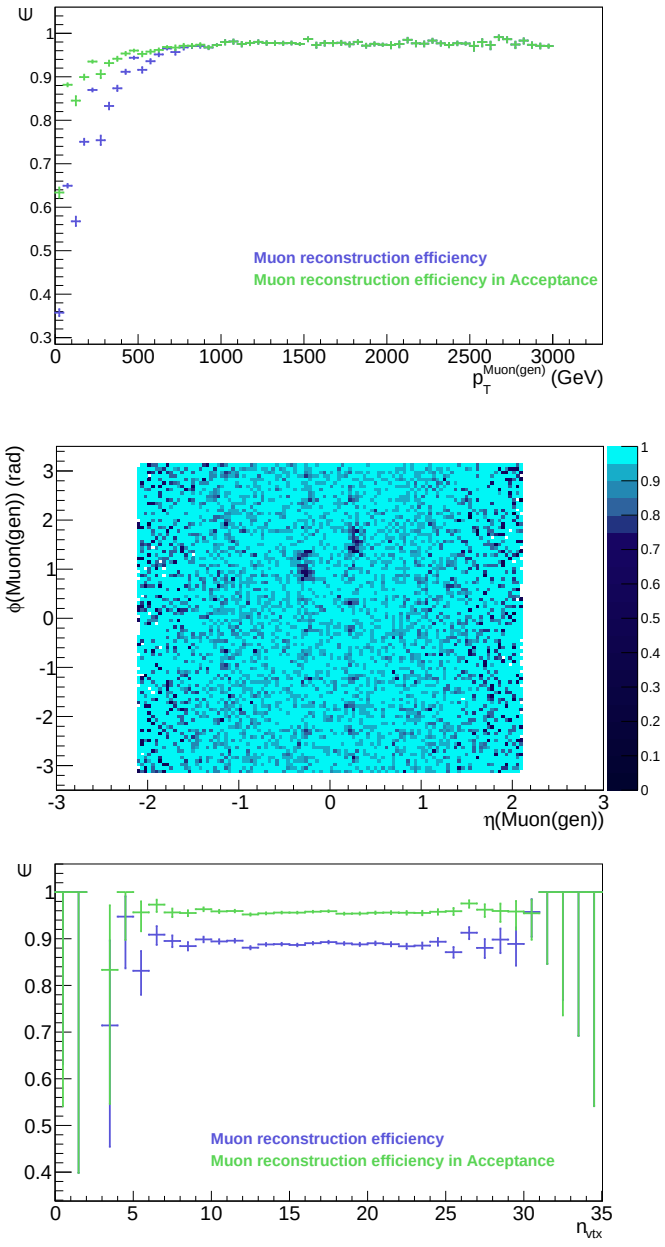

Figure 6: Reconstruction efficiency of muons. For high-p_T muons, the efficiency flattens at around 97% as can be seen in the picture on the top. The acceptance cuts improve the efficiency for low-p_T muons up to 700 GeV severely. In the $\eta-\phi$-distribution (in the middle), the effeciency severely drops at two points, which is to be expected, as there are the supply line for the liquid helium, which the magnet is cooled with. There are (as expected) no features in the Number-of-Vertices plot.

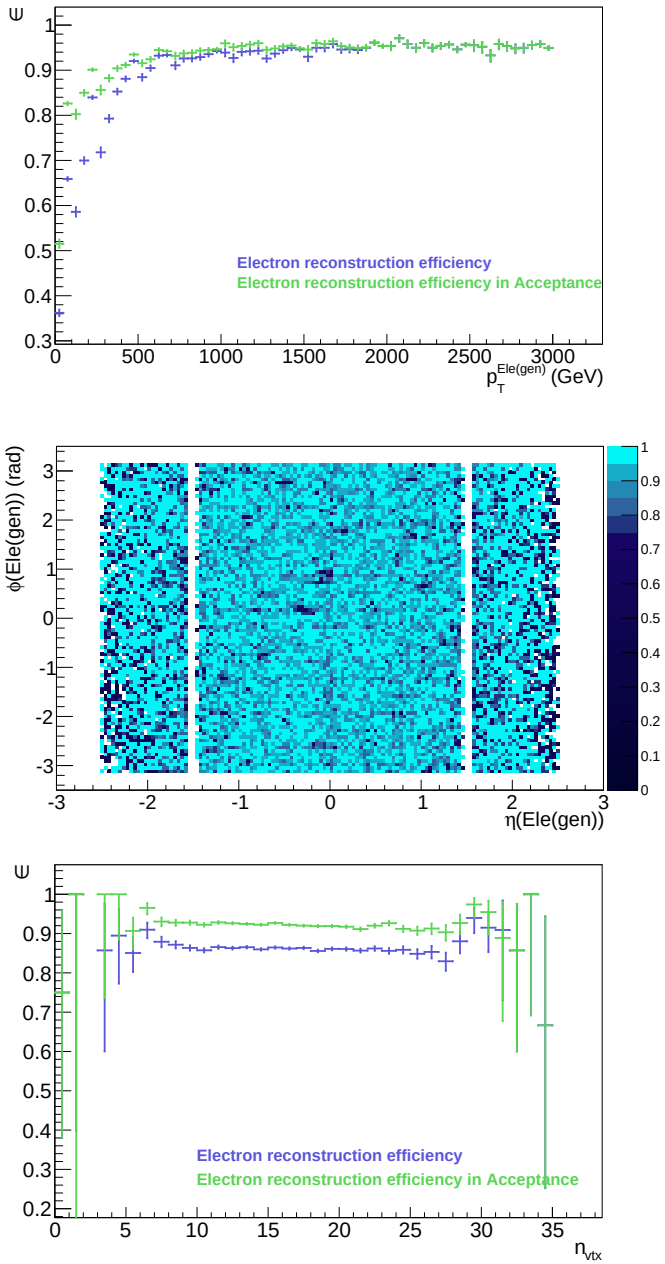

Figure 7: Reconstruction efficiencies for electrons. The efficiency flattens for high-p_T electrons at around 94% (plot on the top). The two gaps in the $\eta - \phi$-plot (in the middle) are the region between barrel and endcap, where electron detection is difficult as there is a gap in the ECAL, and therefore excluded. Also, the Number-of-Vertices distribution shows no features, as expected.

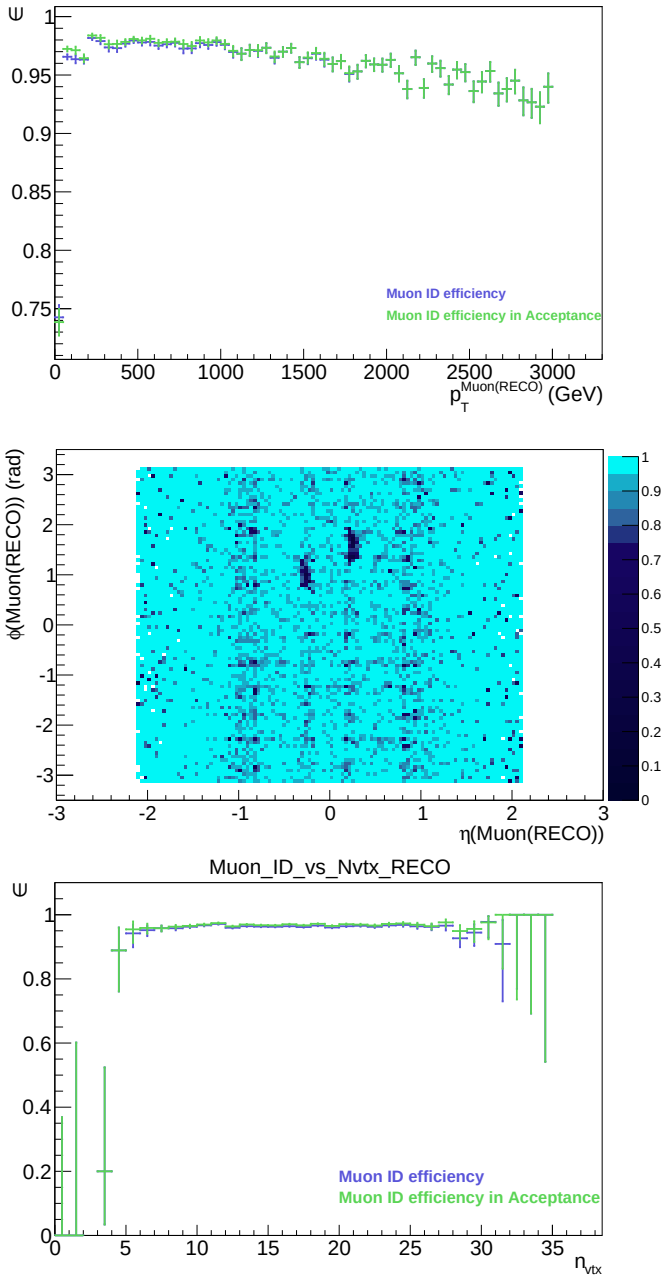

Figure 8: ID efficiency plots for muons. In the top, the efficiency as function of p_T is shown. In the middle, the distribution in dependancy of η and ϕ is seen, and on the bottom, the Number-of-Vertices distribution is shown. The efficiencies have similar characteristics as the ones from the reconstruction (Fig. 6), but the effect of the acceptance cuts is way smaller.

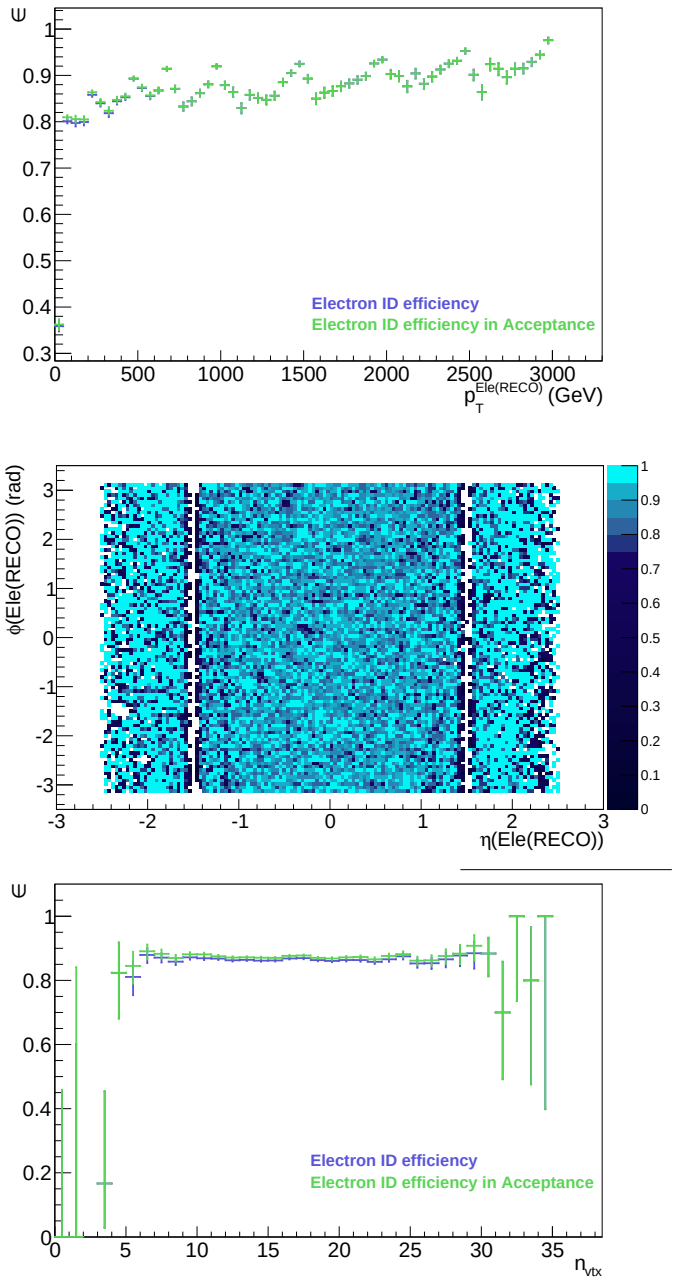

Figure 9: ID efficiencies for electrons. In the top, the efficiency as function of p_T is shown. In the middle, the distribution in dependancy of η and ϕ is seen, and on the bottom, the Number-of-Vertices distribution is shown. The characteristics of the distribution are similar to the ones from reconstruction (Fig. 7), with the acceptance cuts again having close to no influence. The structure in the p_T-distribution is to be expected as the electron is likely to have have the τ-sneutrino mass as momentum, and therefore the ID efficiency increasing for these p_T-values.

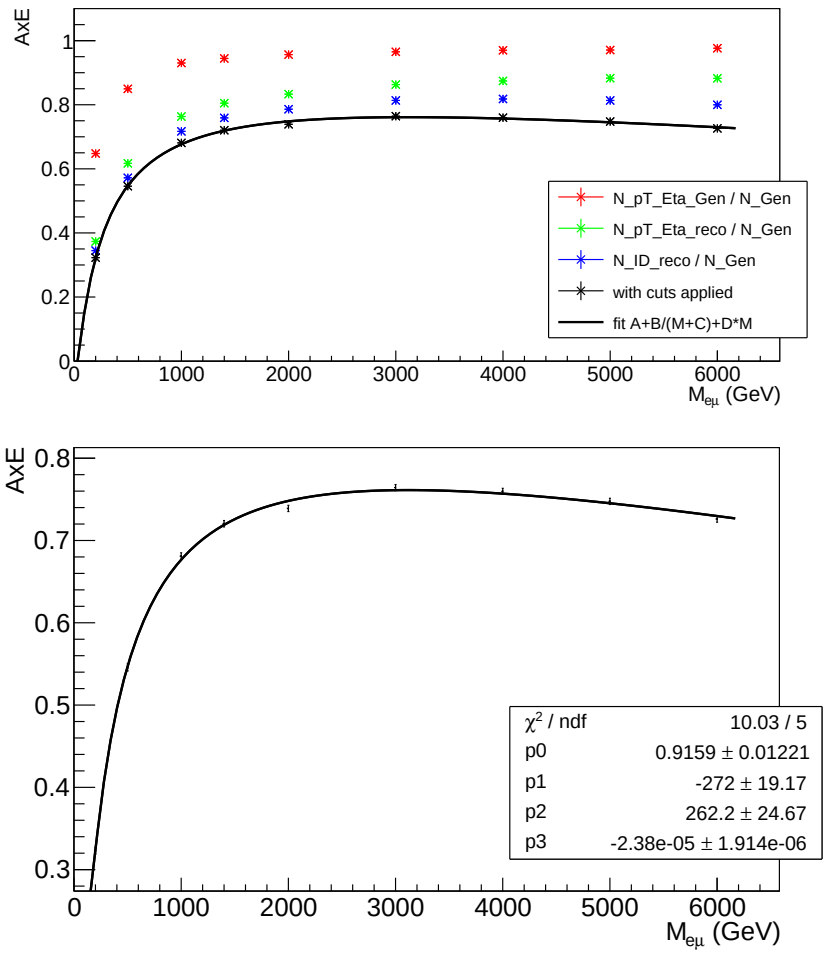

Figure 10: Efficiencies of the different cuts relative to the number of generated events; in red, there is the efficiency of the p_T- and the $\eta-$cut on generated particles. The efficiency for successfull reconstruction is shown in green, while in blue, the ID cuts are applied. In black, the efficiency with additional opposing-sign cut, the b-jet veto and the $\Delta\phi$-cut applied is shown. In the lower diagram, just the fit and the errorbars are shown.

4 Backgrounds and Monte Carlo samples

4.1 Signal and signal Monte Carlo

The signature of the signal is the final state with resonance in the $M_{e\mu}$-spectrum. Here, a τ-sneutrino is created in the annihilation of a down quark with its corresponding antiquark, or similarily the same process with the other down-like quarks. This τ-sneutrino in turn decays into a muon and an electron, a feynman diagram is given in Fig. 3. At the vertices, there are

Name	Generator	No. events	M_{ν_τ}	cross section (pb)
RPVresonantToEMu	CalcHEP	15000	200	585.35
RPVresonantToEMu	CalcHEP	15000	500	27.612
RPVresonantToEMu	CalcHEP	15000	1000	2.0611
RPVresonantToEMu	CalcHEP	15000	1400	0.49332
RPVresonantToEMu	CalcHEP	15000	2000	0.08639
RPVresonantToEMu	CalcHEP	15000	3000	0.0071592
RPVresonantToEMu	CalcHEP	15000	4000	0.00064163
RPVresonantToEMu	CalcHEP	15000	5000	$5.1376 \cdot 10^{-5}$
RPVresonantToEMu	CalcHEP	15000	6000	$3.3123 \cdot 10^{-6}$

Table 4: Private signal samples, created by A. Güth and S. Erdweg. For each τ-sneutrino mass, the generator, number of events, the MC name and the cross section is given. The coupling is given by $\lambda'_{311} = \lambda_{132} = 0.01$.

different possible couplings, in case of this analysis, they are both set to 0.01, but they can be varied aswell (as they are unknown like the τ-sneutrino mass).

All R-Parity violation-signals are samples from the Phys14 run created privately by A. Güth and S. Erdweg, and are listed in Tab. 4. The samples were created for different assumed mass points of the τ-sneutrino and for different couplings, but in this analysis, only the ones with couplings equal to $\lambda'_{311} = \lambda_{132} = 0.01$ are used.

4.2 Backgrounds

In the following section, the most important standard model processes, that also lead to a final state with an electron and a muon, are explained. Additionally it is looked at the most important events that could, by misidentification, result in selected events. All Monte Carlo samples, including the backgrounds from DY, WJets, single top, $t\bar{t}$, WZ and ZZ are taken from the Spring15 MC production campaign and are listed in Tab. 5. As backgrounds, all processes are taken from MC but the jet background, which is estimated with a data driven technique (see Section 4.3). More information on the Monte Carlo generators can be found for Pythia8 [17], Powheg [15], MC@NLO [9].

Name	generator	No. events	binning (GeV)	cross section (pb)
QCD*	Pythia6	9755422	$15 < p_T < 7000$	$8.9731 \cdot 10^{10}$
QCD_MuEnriched	Pythia8	6610000	$15 < p_T < 20$	$1.27319 \cdot 10^{9}$
QCD_MuEnriched	Pythia8	6610000	$20 < p_T < 30$	$5.58528 \cdot 10^{8}$
QCD_MuEnriched	Pythia8	4940000	$30 < p_T < 50$	$1.39803 \cdot 10^{8}$
QCD_MuEnriched	Pythia8	5050000	$50 < p_T < 80$	19222500
QCD_MuEnriched	Pythia8	3880000	$80 < p_T < 120$	2758420.0
QCD_MuEnriched	Pythia8	4030000	$120 < p_T < 170$	469797.0
QCD_MuEnriched	Pythia8	4290000	$170 < p_T < 300$	117989.0
QCD_MuEnriched	Pythia8	4240000	$300 < p_T < 470$	7820.25
QCD_MuEnriched	Pythia8	1930000	$470 < p_T < 600$	645.528
QCD_MuEnriched	Pythia8	1980000	$600 < p_T < 800$	187.109
QCD_MuEnriched	Pythia8	2060000	$800 < p_T < 1000$	32.3486
QCD_MuEnriched	Pythia8	2020000	$1000 < p_T$	10.4305
tW	Powheg	995600	-	38.09
$\bar{t}$W	Powheg	2000000	-	38.09
WW	Pythia8	990000	-	63.21
ZZ	Pythia8	1110000	-	10.32
WZ	Pythia8	990000	-	22.82
DY $\rightarrow$ ll	MC@NLO	30500000	$10 < M_{ll} < 50$	18610.0
DY $\rightarrow$ ll	MC@NLO	28300000	$50 < M_{ll}$	6104.0
$t\bar{t}$	Powheg	19900000	-	730
$W \rightarrow l\nu + x$	MC@NLO	24200000	-	60290

*This QCD sample is used only for the estimation of the jet background (see Ch. 3.3).

Table 5: Official Monte Carlo Samples taken from Spring15 run, with all relevant backgrounds for this search. For each MC the generator, the number of events, the cross section aswell as the possible binning is given.

4.2.1 W boson pair production (WW)

This background is a highly important process for higher invariant masses $M_{e\mu}$ above about 1 TeV and comes from the production of two W bosons, which both decay leptonically. One decays into an electron / positron with its corresponding neutrino, and the other one decays into an muon / antimuon and its corresponding neutrino, as shown in the feynman diagram in Fig. 11. As the neutrinos most likely will not be measured, this process simulates the eμ-final state.

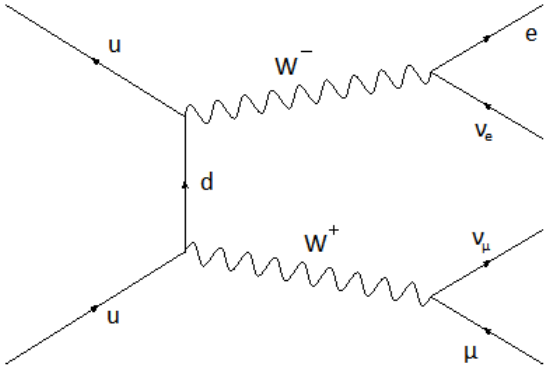

Figure 11: Feynman diagram: W boson pair production. Two W bosons are created and both decay leptonically, resulting in the eμ final state.

4.2.2 Top quark pair production ($t\bar{t}$)

In this process, two top quarks are created, and due to their small lifetime, they decay, before they can hadronize, each to a b quark and a W boson. The b quarks in turn hadronize and the W bosons decay leptonically similar to the WW-background. This background will be the most dominant for invariant eμ-masses below 1 TeV, one exemplary feynman diagram is shown in Fig. 12.

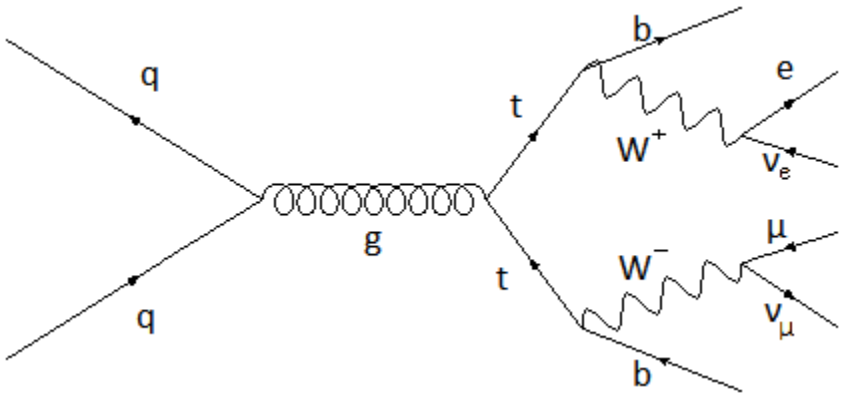

Figure 12: Feynman diagram: Example of $t\bar{t}$-production. A top-antitop pair is created, each of them decaying into a b quark and a W boson. The W bosons decay leptonically and give the eμ final state.

4.2.3 Other diboson production (WZ and ZZ)

Similar to the WW background, interchangeably to the W a Z is produced and then decays into two leptons of the same generation and the W in the lepton and its corresponding neutrino of the other for this analysis relevant generation. These processes are less important than the WW-production as the cross section for Z-production is significantly smaller than the W's one,

aswell as Zs decaying to leptons is way less propable [10]. Two feynman diagrams are given in Fig. 13.

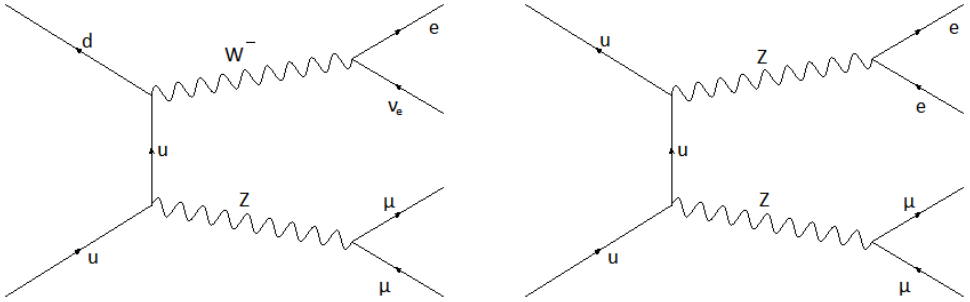

Figure 13: Feynman diagram: Diboson producion (WZ on the left, ZZ on the right). Similar to the WW production, A WZ- or ZZ-pair is created, both decay leptonically and result in the eμ final state (with additional leptons).

4.2.4 Single Top production (tW)

A single top and a W are created. The top quark quickly decays into a bottom quark and a second W. The two W bosons analogously to the WW-production, result in the eμ final state, shown in Fig. 14.

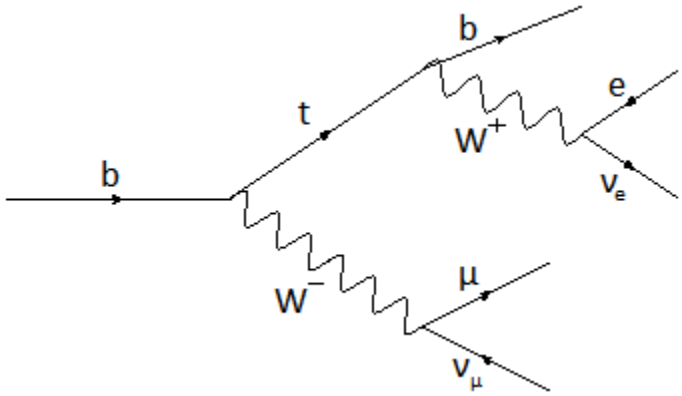

Figure 14: Feynman diagram: Single Top production with eμ final state, where a b quark emits a W and the resulting top also emits a W and both these W bosons decay leptonically.

4.2.5 Drell-Yan process (DY)

The Drell-Yan process describes a hadron-hadron scattering process, where a quark and an antiquark annihilate each other, emitting a virtual photon or a Z boson, which in turn decays into a lepton-antilepton pair. If one of these leptons is misidentified, it is possible to measure the eμ final state, most often this will be the case for a muon misidentified as an electron (as electrons are most likely to be absorbed in the detector and cannot hit the muon chambers).

Another possibility is, that the boson decays into a $\tau\bar{\tau}$-pair, which subsequently decays into an electron (+ neutrinos) and a muon (+ neutrinos). Its feynman diagram is shown on Fig. 15.

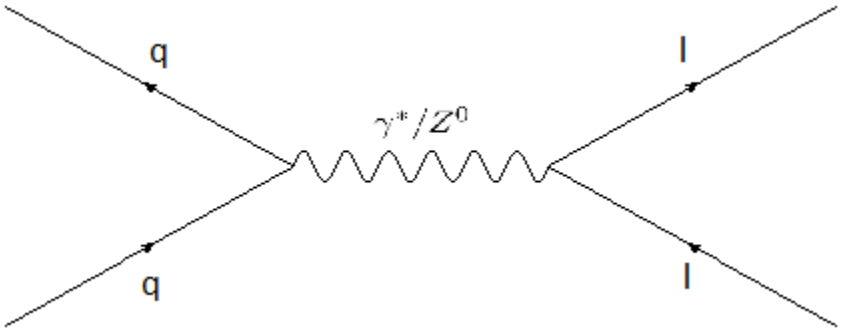

Figure 15: Feynman diagram: Drell-Yan process. Two quarks annihilate and emit a virtual photon or Z boson, which then decays into two leptons.

4.2.6 Jets and multijets (jets)

For backgrounds with jets, a datadriven technique will be used and is simulated with combined backgrounds in the following. These backgrounds come from jets, which occure from quarks which do not decay promptly and therefore (due to the selfcoupling of the gluons) create a whole stream of particles all flying into the same direction. These jets could be misidentified as a lepton in the detector. A possible process would the process taken from quantum chromo dynamics (QCD) shown in Fig. 16 or the W+jets process taken from MC, where the W decays into a muon and its neutrino and the jet fakes an electron, shown in Fig. 17.

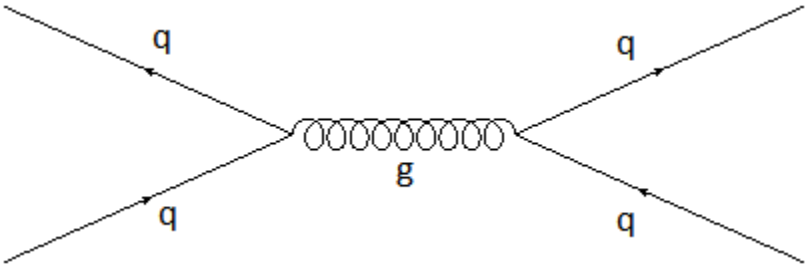

Figure 16: Feynman diagram: QCD process. Two quarks annihilate, emit a gluon which in turn decays into a quark-antiquark pair. Each of these quarks then hadronizes and result in jets.

4.3 Jet Background Estimate

The estimation of the jet background follows closely the procedure done for the 8 TeV data published in [4], though, due to the lack of data, it was modified for this analysis.

In this background, the focus lies on jets, which could be misidentified as electrons or muons, and pass their selection. As the probability for a faked electron is higher than for a faked

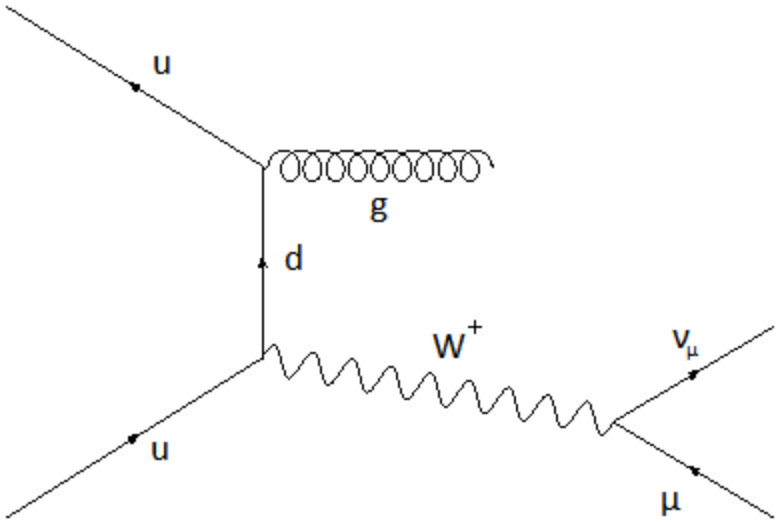

Figure 17: Feynman diagram: W+jets. In this process, a W boson and a gluon are emmited. The W boson decays leptonically (to a muon and a muon neutrino), while the gluon creates a jet, which can be misidentified as an electron.

	barrel		endcap	
	HEEP	PSC	HEEP	PSC
nr. missing hits	≤ 1	≤ 1	≤ 1	≤ 1
H / E	< 0.05	< 0.15	< 0.05	< 0.1
$\sigma_{i\eta i\eta}$	—	< 0.013	< 0.03	< 0.034
|dxy|	< 0.02	< 0.02	< 0.05	< 0.05

Table 6: The selection requirements for starting point of fake rate calculation in comparison to their corresponding HEEP values, PSC stands for preselection cuts, which are used to evaluate the jet background

muon, the latter is neglected. The fake rate is defined by the number of electrons passing the HEEP-selection (defined in Section 3.1.2) over the number of electrons passing the fake rate preselection cuts, which are taken from the Z' search from the 8 TeV analysis shown in Tab. 6 [7]. As there are no data for the 2015 run, this fake rate is determined on events, where no muons are evident. Due to this, the muon-enriched QCD sample are not viable for his method, because this background has low statistics for this method by design. Therefore, for this part, an additional QCD sample is used (see Tab. 5). In search of a parametrisation of the fake rate, it is plotted agains E_T, η and ϕ. The results are shown in Fig. 18 and 19 and the parametrisation is given in Eq. 10.

$$FakeRate = \begin{cases} 0.00297 & \text{for } \eta < 1.442 \\ -0.0511 + 0.0443 \cdot \eta & \text{for } 1.56 < \eta < 2.5 \end{cases} \tag{10}$$

This result is in the same scale as the result from 8 TeV, though there a dependancy on E_T

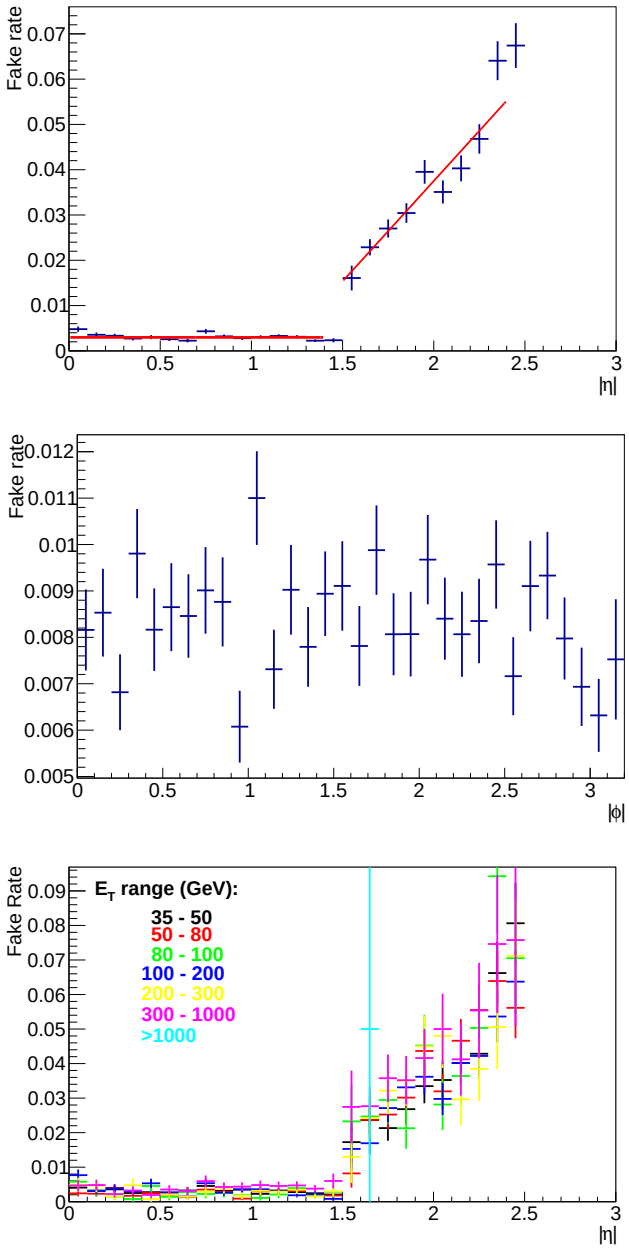

Figure 18: Fake Rate estimation results. The fake rate is flat in the barrel and linear in the endcap (top). There do not seem to be dependancies on ϕ (middle). In order to test if there are dependancies on E_T, the $\eta-$plot is done for several E_T-bins, but there are no dependancies to be seen either (the statistic for $E_T > 1000$ GeV is too small to make a point on it, bottom). The parametrisation is given in Eq. 10.

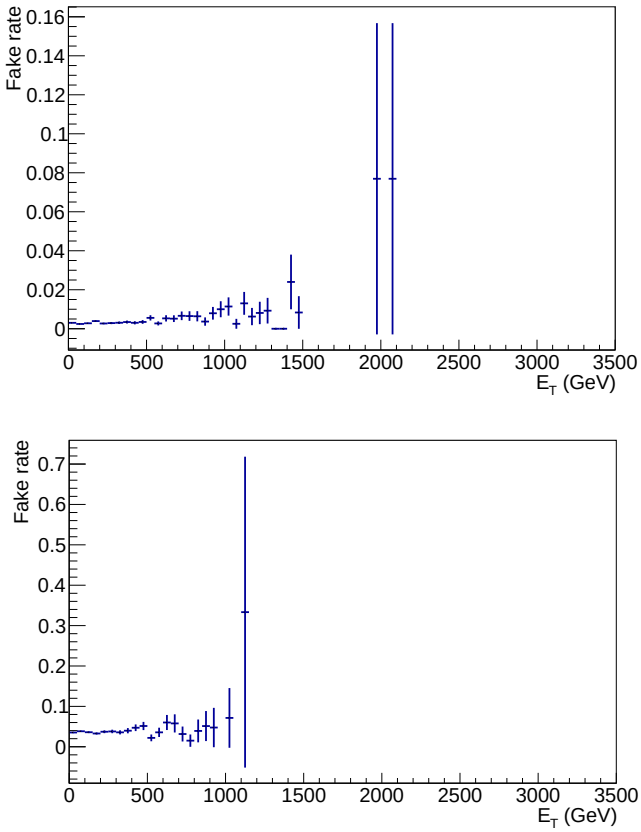

Figure 19: Fake Rate estimation results. The fake rate as a function of the transversal energy is plotted. On the top, the distribution for the barrel is seen, while on the bottom, the distribution for the endcap can be seen.

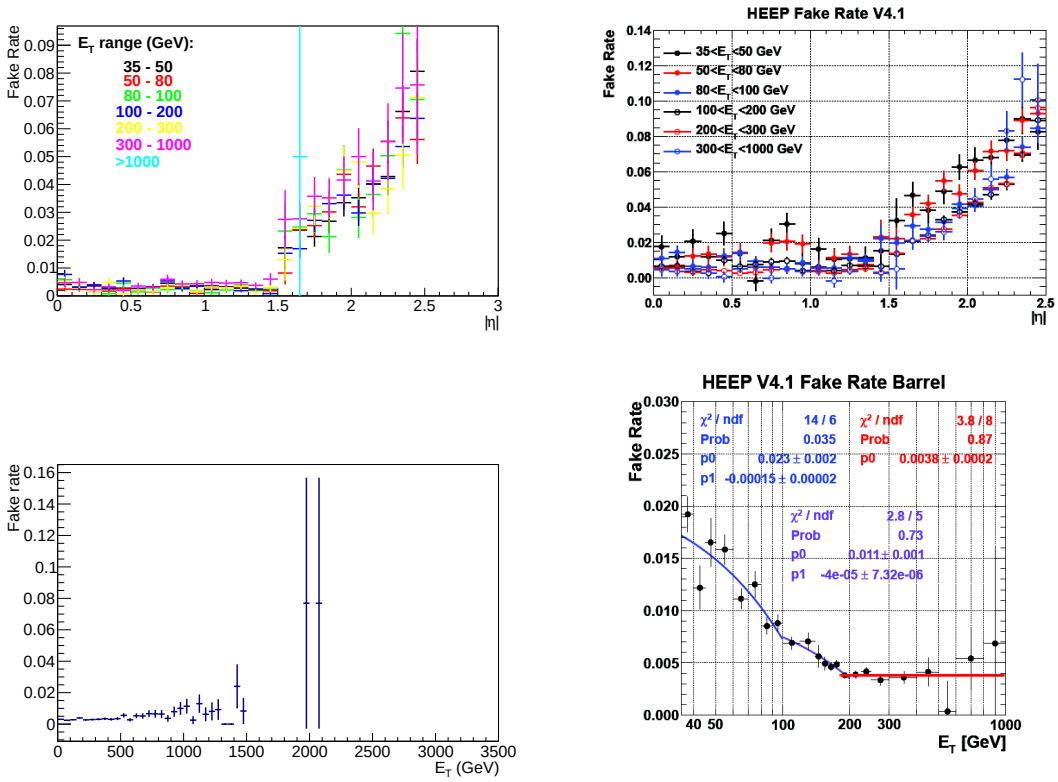

Figure 20: Results for Fake Rate estimation: Comparison between 8 TeV analysis and result from the method mentioned above. In the top, there are the plots for the η-dependancy, in the bottom the transversal energy in the barrel (on the left are plots from this analysis, on the right there are plots from 8 TeV analysis). As can be seen, in the 8 TeV analysis, a dependancy on the transversal energy was found and stated, while for this analysis, no dependancy on E_T is used.

was stated [7]. Two plots for comparison are shown in Fig. 20. The plateau in the barrel is in the analysis from 8 TeV slightly higher, but the increase of the fake rate in the endcap is slightly lower.

In order to get an estimation of the jet background, the fake rate is then applied to events with at least one muon passing the full selection and the electron passing the preselection cuts but not the full electron ID selection. Events, where such fake electrons are evident, are additionally reweighted, in order to compensate for the lost electrons from the requirement, that these electrons have to fail the full selection. As those events still carry a significant contribution from $t\bar{t}$, DY and WW production, they have to be subtracted from the MC samples in order to avoid double counting. In order to validate the method, the result is compared to the number of eμ events in the QCD background, which should be in the same scale, as most of the events from QCD have jets, which could fake electrons. Additionally, the fake rate method is compared to the W+jets background from MC which also should be of the same size. This is shown in Fig. 21.

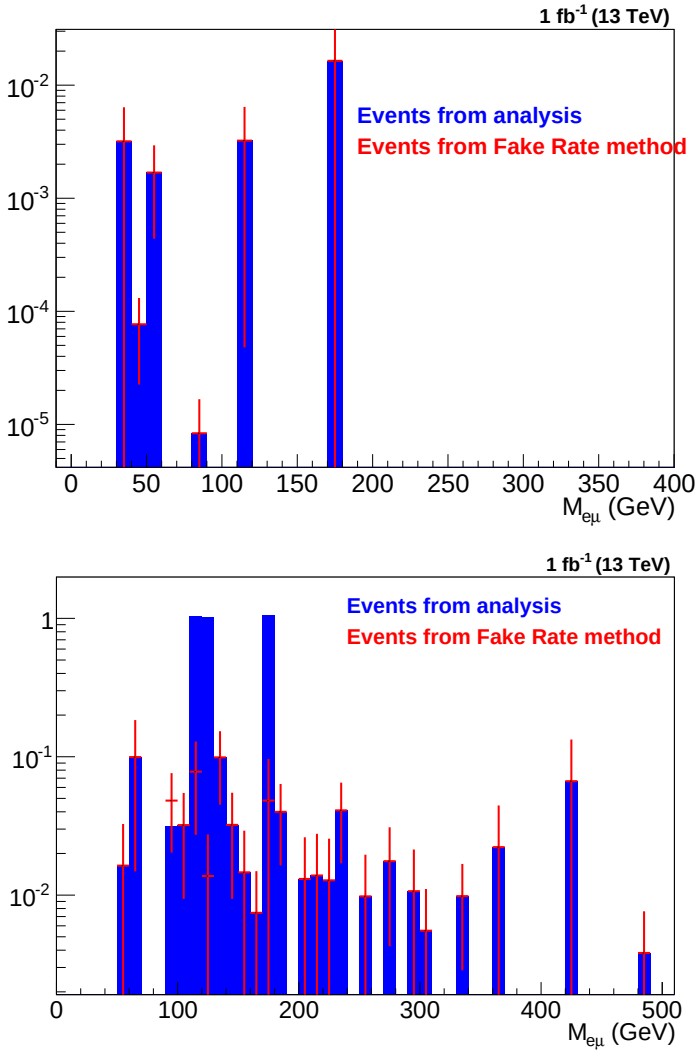

Figure 21: Closure Test: As effectively all events from QCD-samples have only jets, which could fake electrons, it is expected for the number of resonances be of the same size as the number of jets detected via the fake rate method. This statement holds true for the W+jets sample aswell. On the top, there is the closure test for the QCD-samples, on the bottom for the W+Jets sample. It can be seen that the agreement between data and fake rate method is very good.

4.4 Data sample

Due to the fact, that there is no data sample available at the time of creation of this analysis, all backgrounds (from Tab. 5) are merged, but the one used only for the jet background estimation, and taken as pseudodata.

5 eμ invariant mass resolution

In the following section, the invariant mass resolution of the eμ pair is studied. The ideal muon alignment is used, in case of other alignements, the resolution would worsen [4]. The relative mass resolution is defined by $(M_{e\mu}^{reco} - M_{e\mu}^{gen})/M_{e\mu}^{gen}$ and is evaluated for all events that are selected in the MC signal samples.

On the resulting distributions, Gaussians are fitted on the distribution mean ± the RMS of the distribution. As it can be seen, due to the non-Gaussian tails, which inherit from bremsstrahlung and misreconstruction, the fits do not seem to describe the core of the distribution properly. Therefore, an additional fit is done for each distribution, whereas now, it is fitted on the mean from the gaussian fit ± 1.8 times the RMS from the gaussian fit. This is shown in Fig. 22. Obviously, the width of the distribution differs with different masses, so the resolution is then plotted against the invariant mass of the eμ pair, shown in Fig. 23, where it can be seen, that the resolution becomes worse with higher invariant masses. This comes from the fact, that the muon resolution also becomes worse with higher muon-p_T, as the bend of the trajectory is less exactly determinable. To show this, the muon momentum resolution $(1/p_T^{reco} - 1/p_T^{gen}) \cdot p_T^{gen}$ and the electron momentum resolution $(p_T^{reco} - p_T^{gen})/p_T^{gen}$ are also shown in Fig. 23. The electron resolution becomes better with higher p_T due to the fact that the calorimeter gets stronger signals, up to a point where it saturates and the resolution flattens, where the muon resolution worsens, as it is harder to evaluate its transversal momentum from a less bend track.

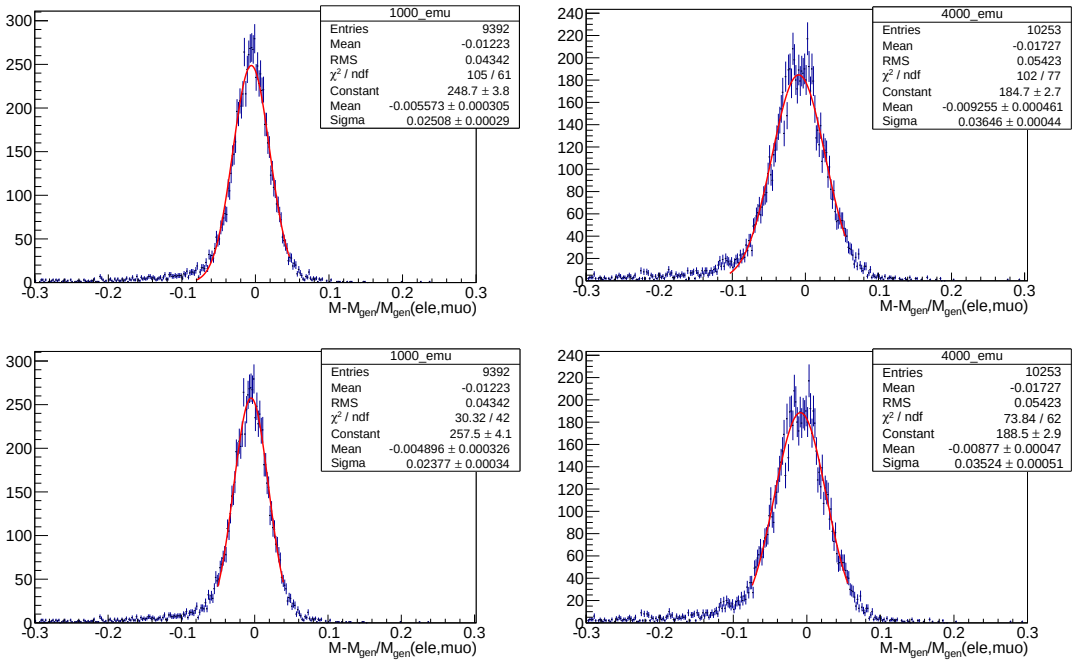

Figure 22: Mass resolution graphs with gaussian fits. In the upper pictures, the function is fitted on the distribution mean ± distribution RMS, while in the lower ones, the gaussian is fitted on the previous fit mean and 1.8 times its RMS. In the comparison of the $M_{e\mu} = 1000$ GeV sample pictures and the $M_{e\mu} = 4000$ GeV , a significant increase in the width of the distribution can be seen.

Additionally, a function is fitted at the resolution in order to determine the resolution for arbitrary mass points, which is necessary for the limit setting procedure. As the second gaussains described the core of the distribution more precisely, this function is used:

$$\frac{\sigma(\mathrm{M}_{e\mu})}{\mathrm{M}_{e\mu}} = 0.039 - \frac{38.12}{1341 + \mathrm{M}_{e\mu}/\mathrm{GeV}} + 1.15 \cdot 10^{-6}\mathrm{M}_{e\mu}/\mathrm{GeV} \tag{11}$$

In comparison the the results from 8 TeV analysis, there is a slight improvement on the resolution of about 0.5 % relative to the 2012 C2 alignement [4], shown in Fig. 24.

6 Invariant mass

The invariant mass distribution after full selection is shown in Fig. 25. As there are no data for 13 TeV collisions at this point in time, all backgrounds are taken from simulation and, scaled to their cross section given in Tab. 5, merged in order to get pseudodata. The single backgrounds are also scaled to their cross section, except for the jet background, which is estimated as descibed in Section 4.3. The distribution is additionally evaluated for opposite-sign electric charge (of the leptons) events only, and is shown in Fig. 26 (left) together with the distribution for opposite-charge events where the $\Delta\phi < 2.7$ cut aswell as the b-Jet veto is applied.

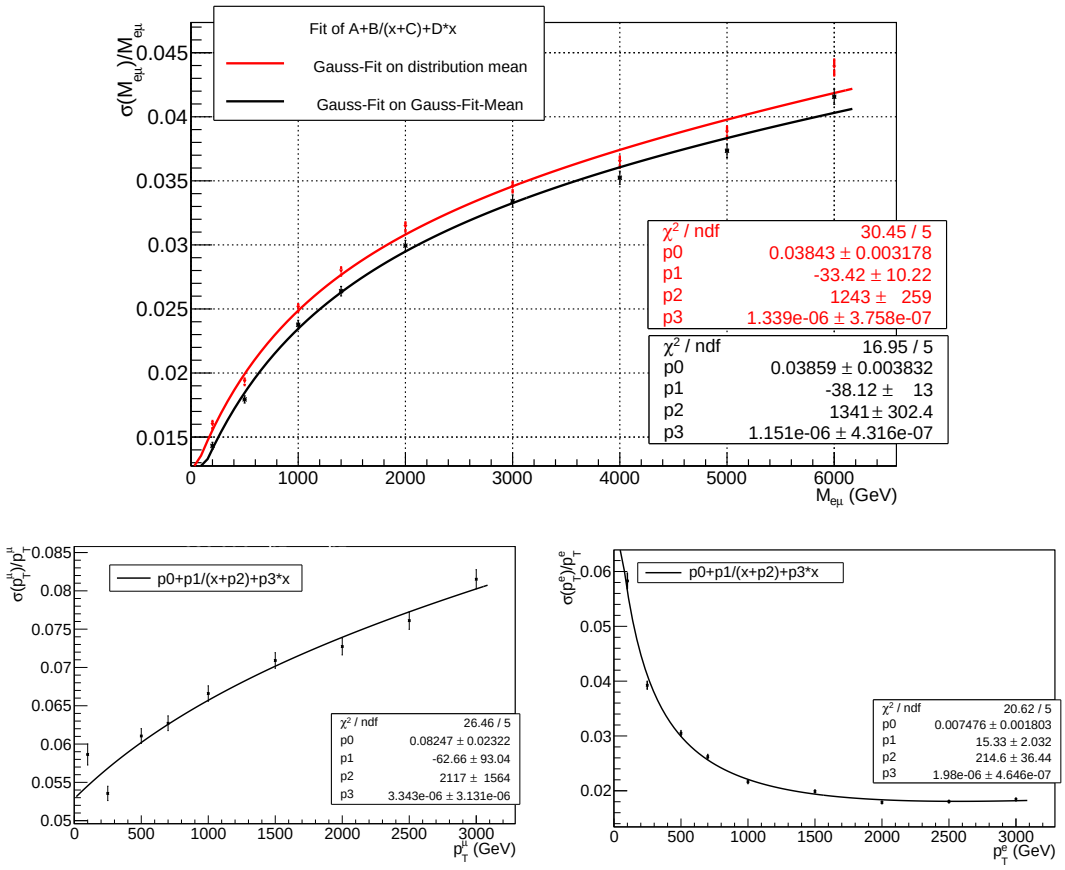

Figure 23: Resolution as a function of $M_{e\mu}$ (on the top) and corresponding momentum resolutions of the leptons. The electron resolution (on the bottom right) increases with its p_T due to better signals from the calorimeters, but as they saturate, this resolution flattens. The muon resolution (on the bottom left), whose influence dominates the mass resolution for high p_T, worsens for higher p_T, as its momentum is evaluated from the bend of the trajectory, which becomes less bend for higher p_T.

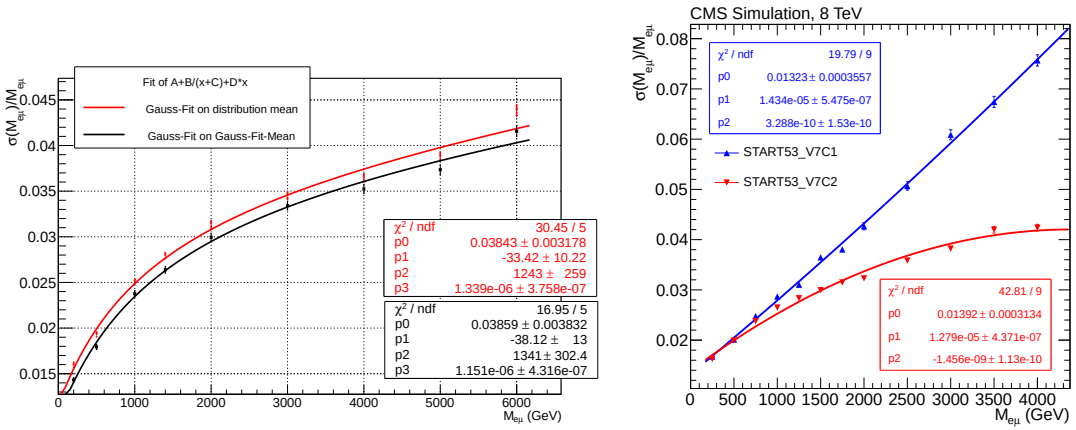

Figure 24: Comparison of invariant mass resolution from 8 TeV analysis (on the right) to this analysis (on the left). It can be seen, that the resolution was slightly enhaced relative to the C2 alignment.

The background composition is shown in Tab. 7. For the whole range of invariant masses $M_{e\mu}$ the background is dominated by $t\bar{t}$ events, followed by tW for $M_{e\mu} < 600$ GeV. For higher invariant masses, the WW becomes more important. The Drell-Yan background is mainly relevant around the Z mass and loses importance for higher invariant masses. The other Diboson processes as well as the jet background only give a small contribution to the whole background.

Process	$M_{e\mu} < 200$ GeV	200 GeV $< M_{e\mu} <$ 600 GeV	600 GeV $< M_{e\mu}$
$t\bar{t}$	80%	79%	70%
WW	4%	5%	19%
tW	10%	13%	10%
DY	4%	1%	<1%
WZ, ZZ	1%	1%	-
Jets	1%	1%	<1%

Table 7: Background composition accoring to simulation

7 Statistical Interpretation

The RPV signal results in a narrow resonance, so its width Γ is small compared to the detector resolution. As the signal's tails from radiation are small, a single Gaussian with parameters M and σ is used as the signal model. Here, the σ is taken from the invariant mass resolution (Eq. 11). As input for the limit setting tool, histograms are used, which are taken from the signal probability density function and normalized to the expected number of signal events. This number is given by the luminosity (1 fb^{-1}), the efficiency from the fit to acceptance times efficiency (Eq. 9) and the cross section from simulation [4]. No systematic uncertainties are

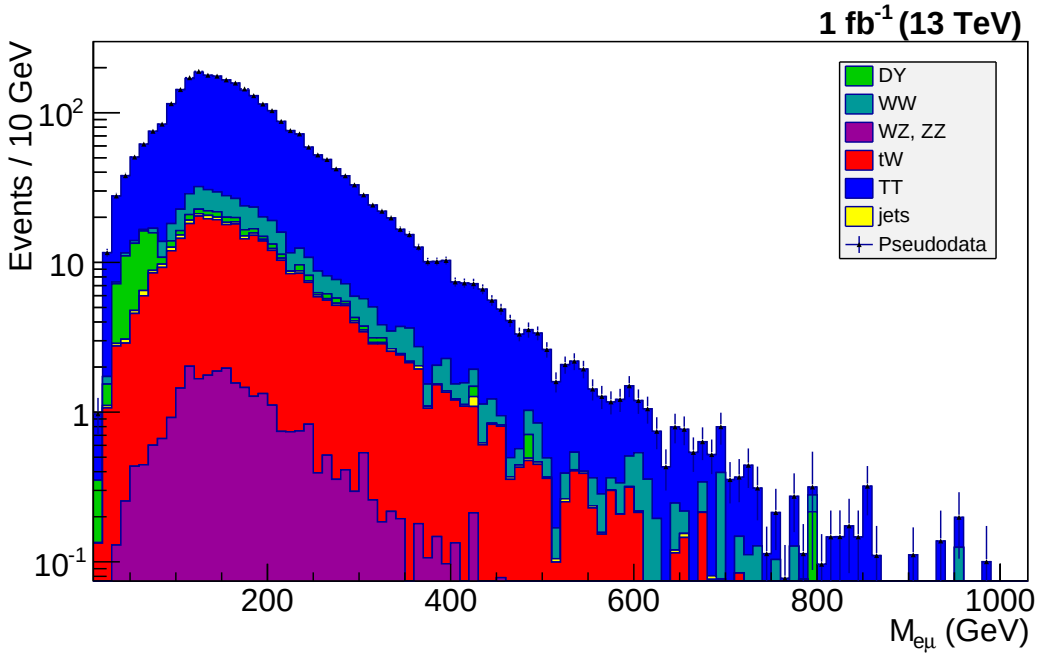

Figure 25: Final eμ mass distribution, as can be seen, the $t\bar{t}$-background is the dominating one for the whole mass spectrum, the WW-background becomes more important for higher masses. Drell-Yan events mainly contribute at the Z-mass, otherwise it is a small background. There are events with an invariant mass of up to 1 TeV.

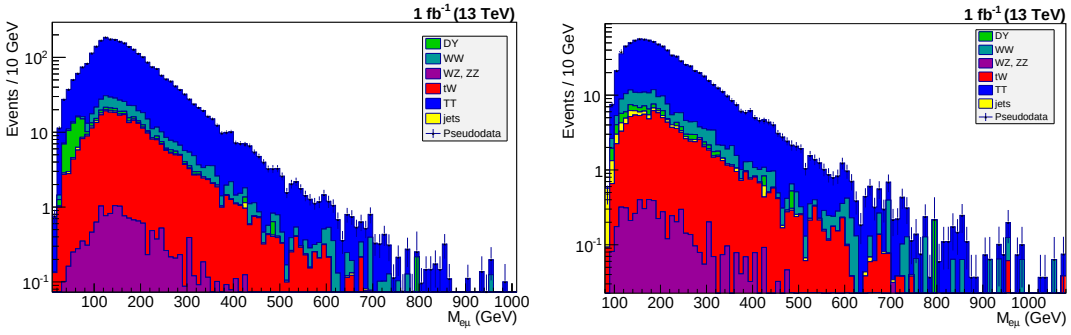

Figure 26: Eμ mass distribution for opposite charge events (left), and with b-Jet veto and $\Delta\phi < 2.7$ cut applied (right). The latter mainly supress the DY background and reshape the whole distribution slightly.

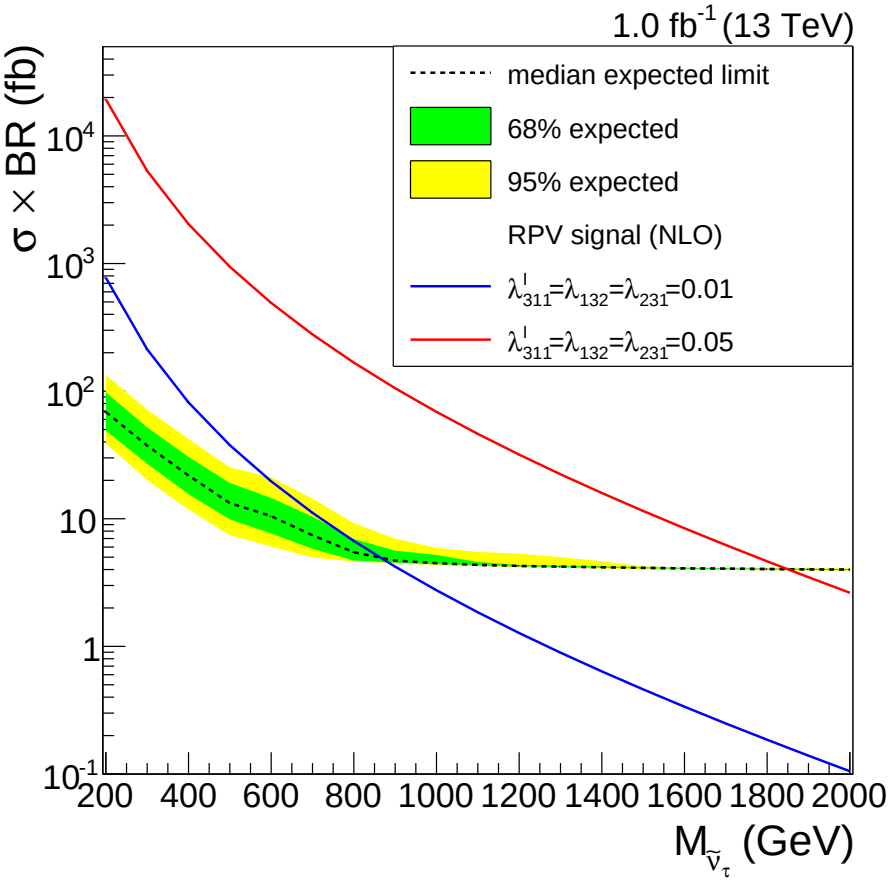

Figure 27: 95% CL expected limit on the signal cross section times branching ratio for the signal as a function of the resonance mass. The cross section of the RPV model with couplings $\lambda'_{311} = \lambda_{132} = 0.01$ is given by the blue line.

included.

Assuming, no signal can be seen in data from runs at 13 TeV, a limit can be set on the mass of the τ-sneutrino. The expected limit at confidence level (CL) 95% on the signal cross section is determined with the limit setting tool developed by the Higgs group [19]. For the signal cross section, the Markov-Chain Monte Carlo Bayesian method is used. For this method, a prior distribution for the unknown parameters is needed. This distribution is assumed to be constant, as there is no information available for it [5].

The expected 95% CL limit on the signal cross section times branching ratio for the resonance signal shape are shown in Fig. 27. The theory cross section for the couplings $\lambda'_{311} = \lambda_{132} = 0.01$ is evaluated and shown in blue. The RPV signal model can be excluded at 95% CL for $M_{\tilde{\nu_\tau}} < 910$ GeV. A previous exclusion limit has been 1280 GeV from CMS at 8 TeV[4].

8 Conclusion

The search for a supersymmetric process giving an electron and a muon in the final state has been carried out with Monte Carlo generated pseudodata. The efficiencies of the different cuts applied have been estimated and discussed. As backgrounds, the Diboson processes, the $t\bar{t}$-production, the Drell-Yan process and the single top process were considered and taken from MC. Additionally, the jet background was estimated using a datadriven technique. In the assumption that nothing is seen, new limits have been set on the resonant production of τ-sneutrinos in RPV SUSY with subsequent decay into a eμ pair for 13 TeV. With couplings $\lambda'_{311} = \lambda_{132} = 0.01$, this scenario has been excluded for masses $M_{\tilde{\nu_\tau}}$ below 910 GeV for a integrated luminosity of 1 fb^{-1}. Several comparisons to 8 TeV analysis have been done.

References

[1] http://www.lhc-facts.ch/index.php?page=cms.

[2] The nobel price in physics 2004. www.nobelprize.org/nobel_prizes/physics/laureates/2004/popular.html, October 2004.

[3] Standard model of elementary partilces. https://upload.wikimedia.org/wikipedia/commons/0/00/Standard_Model_of_Elementary_Particles.svg, June 2006.

[4] Thomas Reis Andreas Gueth, Emmanuel Olaiya. Search for Lepton Flavor Violating Decays of Heavy States to electron / muon Pairs in pp Collisions at a centre of mass energy of 8 TeV. *CMS Draft note*, February 2015.

[5] Bradley P. Charlin and Siddharta Chib. Bayesian Model Choice via Markov Chain Monte Carlo Methods, 1995. Journal of the Royal Statistical Society. Series B (Methodological) Vol. 57, No. 3 (page 473-484).

[6] CMS Collaboration. The CMS experiment at the CERN LHC. iopscience.iop.org/1748-0221/3/08/S08004/pdf/1748-0221_3_08_S08004.pdf, August 2008. JINST S08004 (2008).

[7] B. Clerbaux et al. Update of the Z' -> ee analysis with Jan 22 re-recoed data, 2013. CMS Note: CMS AN-2013/359.

[8] G. Abbiendi et al. Muon Reconstruction in the CMS Detector, 2008. CMS Note: CMS AN-2008/097.

[9] J. Alwall et. al. The automated computation of tree-level and next-to-leading order differential cross sections, and their matiching to parton shower simulations. http://arxiv.org/abs/1405.0301, 2014. JHEP 07 (2014) 079.

[10] J.Beringer et al. (Particle Data Group). Particle physics booklet, 2012. Phys. Rev. D86, 010001.

[11] David Griffiths. *Introduction to Elementary Physics*. WILEY-VCH, 2010. Second, Revised Edition.

[12] Johannes Haase. *Study of the electron -> photon misidentification rate in the ATLAS detector*. January 2011. http://atlas-archiv.desy.de/theses/Haase_dipl.pdf.

[13] Sam Harper. HEEP Electron ID and Isolation. https://twiki.cern.ch/twiki/bin/viewauth/CMS/HEEPElectronID, June 2015.

[14] Gordon Kane. *supersymmetry - unveiling the ultimate laws of nature*. Perseus Publishing, 2000.

[15] G. Ridolfi S. Fricione, P. Nason. Heavy-quark pair production. http://arxiv.org/abs/0707.3088, 2007. JHEP 0709 (2007) 126.

[16] Daneile Trocino. Baseline muon selections for Run-II MC. https://twiki.cern.ch/twiki/bin/view/CMS/SWGuideMuonIdRun2#HighPT_Muon, june 2015.

[17] P. Skands T.Sjoestrand, S. Mrenna. A Brief Introduction to PYTHIA 8.1. `http://arxiv.org/abs/0710.3820`. Comput.Phys.Commun.178:852-867,2008.

[18] C. Wiebusch. Skript zur Vorlesung "Experimentalphysik Vb: Teilchen- und Astrophysik", 2014. RWTH Aachen, WS 2014/15.

[19] Higgs working group. Higgs combined limit setting tool. `https://twiki.cern.ch/twiki/bin/view/CMS/SWGuideHiggsAnalysisCombinedLimit`.